

Published in final edited form as:

*Acc Chem Res.* 2009 July 21; 42(7): 948–957. doi:10.1021/ar800237f.

## Responsive MRI agents for sensing metabolism *in vivo*

Luis M. De Leon-Rodriguez<sup>1</sup>, Angelo Josue M. Lubag<sup>1</sup>, Craig R. Malloy<sup>1,2,3,4</sup>, Gary V. Martinez<sup>5</sup>, Robert J. Gillies<sup>5</sup>, and A. Dean Sherry<sup>1,2,6</sup>

<sup>1</sup>Advanced Imaging Research Center, University of Texas Southwestern Medical Center, Dallas, TX 75235

<sup>2</sup>Department of Radiology, University of Texas Southwestern Medical Center, Dallas, TX 75235

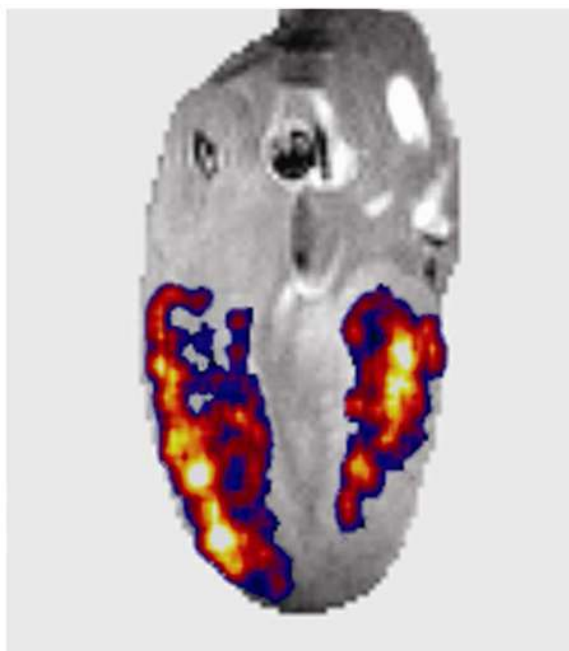
<sup>3</sup>Department of Internal Medicine, University of Texas Southwestern Medical Center, Dallas, TX 75235

<sup>4</sup>VA North Texas Health Care System, Dallas, TX 75216

<sup>5</sup>Department of Biochemistry and Molecular Biophysics, Arizona Cancer Center, University of Arizona, Tucson, AZ and the H. Lee Moffitt Cancer Center & Research Institute, Tampa, FL 33612

<sup>6</sup>Department of Chemistry, University of Texas at Dallas, Richardson, TX 75083

## CONSPECTUS



Magnetic resonance imaging (MRI) has inherent advantages in safety, three-dimensional output, and clinical relevance when compared with optical and radiotracer imaging methods. However, MRI contrast agents are inherently less sensitive than agents used in other imaging modalities primarily because MRI agents are detected indirectly by changes in either the water proton relaxation rates ( $T_1$ ,  $T_2$ , and  $T_2^*$ ) or water proton intensities (chemical exchange saturation transfer and paramagnetic chemical exchange saturation transfer, CEST and PARACEST). Consequently, the detection limit of an MRI agent is determined by the characteristics of the background water signal; by contrast, optical and radiotracer-based methods permit direct detection of the agent itself. By virtue of responding to background water (which reflects bulk cell properties), however, MRI contrast agents have considerable advantages in "metabolic" imaging—that is, spatially resolving tissue variations

in pH, redox state, oxygenation, or metabolite levels. In this Account, we begin by examining sensitivity limits in targeted contrast agents and then address contrast agents that respond to a physiological change; these responsive agents are effective metabolic imaging sensors.

The sensitivity requirements for a metabolic imaging agent are quite different from those for a targeted  $\text{Gd}^{3+}$ -based  $T_1$  agent (for sensing cell receptors, for example). Targeted  $\text{Gd}^{3+}$  agents must have either an extraordinarily high water proton relaxivity ( $r_1$ ) or multiple  $\text{Gd}^{3+}$  complexes clustered together at the target site on a polymer platform or nanoparticle assembly. Metabolic MRI agents differ in that the high relaxivity requirement, although helpful, is eased because these agents respond to bulk properties of tissues rather than low concentrations of a specific biological target. For optimal sensing, metabolic imaging agents should display a large change in relaxivity ( $\Delta r_1$ ) in response to the physiological or metabolic parameter of interest.

Metabolic imaging agents have only recently begun to appear in the literature and only a few have been demonstrated *in vivo*. MRI maps of absolute tissue pH have been obtained with  $\text{Gd}^{3+}$ -based  $T_1$  sensors. The requirement of an independent measure of agent concentration in tissues complicates these experiments, but if qualitative changes in tissue pH are acceptable, then these agents can be quite useful. Finally, we describe examples of imaging extracellular pH in brain tumors, ischemic hearts, and pancreatic islets with  $\text{Gd}^{3+}$ -based pH sensors and discuss the potential of CEST and PARACEST agents as metabolic imaging sensors.

## Introduction

Magnetic resonance imaging is a spectacular tool for providing high resolution anatomical images of rodents and humans but is markedly less sensitive than optical or radiotracer imaging modalities for most molecular imaging applications. However, it could be argued that the potential for MRI at a molecular level is equally exciting and it offers the inherent advantages of safety, three dimensional imaging, and high clinical relevance. Most chemists are familiar with small molecule MRI agents that alter image contrast by changing either the  $T_1$  or  $T_2$  of tissue water but many may not be aware of the limitations of such agents for molecular imaging *in vivo*.  $\text{Gd}^{3+}$ -based agents are widely accepted by clinicians because they are easy to administer and they provide positive contrast (imaging brightening) in anatomical images rather than negative contrast (image darkening). Currently available agents consist of low molecular weight  $\text{Gd}^{3+}$  chelates that distribute into all extracellular space.<sup>1–3</sup> For this reason, these agents produce a general brightening of all tissues in proportion to the extracellular space of each tissue. The standard clinical injection dose of a  $\text{Gd}^{3+}$  contrast agent is 0.1 mmol/kg and, depending upon variations in the extracellular space of various tissues, this corresponds to an average extracellular tissue concentration of about 0.5 mM. Given a typical relaxivity of 4  $\text{mM}^{-1}\text{s}^{-1}$  for a clinical  $\text{Gd}^{3+}$ -based agent, this corresponds to an increase in  $T_1$  relaxation rate of 2  $\text{s}^{-1}$ , a value that is easily detected at common imaging fields. Rooney, *et al.*<sup>4</sup> have demonstrated that extracellular contrast agents are easier to detect at higher magnetic fields due to an increase in tissue water  $T_1$ , an important consideration as clinical imaging moves to higher fields. This indicates that lower doses of contrast agent will be equally effective at higher imaging fields. The detection limit of a targeted  $\text{Gd}^{3+}$ -based  $T_1$  agent is less easily predicted because local tissue contrast depends upon many factors including the imaging pulse sequence, pixel size, water access to the  $\text{Gd}^{3+}$  complex at the targeted site, and the relaxivity of the targeted agent *in vivo*. Although accumulation of low molecular weight chelates in the extracellular space is sensitive to many diseases, the process is nonspecific and insensitive to many normal physiological processes regardless of imaging field.

The motivation for developing new MRI contrast agents is to add molecular, physiological or biochemical specificity to routine anatomical imaging. Numerous *in vitro* examples of  $T_1$  or  $T_2$  responsive MR agents have been reported but only a few have been demonstrated to work

*in vivo*. The classic example of a responsive  $T_1$  agent first reported by Moats, Fraser and Meade<sup>5</sup> was later demonstrated to respond as anticipated after injection into *X. laevis* embryos.<sup>6</sup> Perez, *et al.*,<sup>7</sup> later demonstrated the use small particulates of iron oxide as a platform for magnetic resonance  $T_2$  switches -this technology continues to evolve in a number of laboratories.<sup>8–10</sup> Superparamagnetic iron-oxide nanoparticles have also been investigated for targeting tumors and tracking stem cells but these agents typically do not “respond” to their local tissue environment or to physiology and hence have not been applied to metabolic imaging *in vivo*.<sup>11</sup> The goal of this short review is to address the question of sensitivity limits and options for  $T_1$  shortening agents for molecular targeting and to compare those requirements with those of physiologically responsive agents to measure metabolic events *in vivo*.

## The detection limit of targeted $Gd^{3+}$ -based $T_1$ agents – how much does one need?

If one were to ask users what they think the detection limit of a typical  $Gd^{3+}$ -based  $T_1$  agent would be, one would get widely diverse answers ranging from ~500  $\mu M$  (0.5 mM) to perhaps as low of 50  $\mu M$ . We recently addressed this question systematically to determine that the lower detection limit of a low molecular weight GdDOTA-peptide having an unbound (non-targeted) solution relaxivity ( $r_1$ ) of 10.7  $mM^{-1}s^{-1}$  was  $9 \pm 3 \mu M$ .<sup>12</sup> Upon binding of this  $Gd^{3+}$ -peptide conjugate to its receptor localized on agarose beads, the relaxivity of the agent increased to 17  $mM^{-1}s^{-1}$  and its detection limit dropped to  $4 \pm 1 \mu M$ . These experiments allowed us to predict the lower detection limits of other molecularly targeted  $Gd^{3+}$  complexes, coming to the conclusion that if a targeted  $Gd^{3+}$  complex had a fully-bound relaxivity of 100  $mM^{-1}s^{-1}$ , it should be detectable if the concentration of its target receptor molecule was 690 nM. A relaxivity value of 100  $mM^{-1}s^{-1}$  has proven difficult to achieve for  $Gd^{3+}$ -polyamino-polycarboxylate complexes having a single water exchange site. One could consider using one of the novel fast water exchange systems designed by Raymond, *et al.* with predicted motionally restricted relaxivities ranging from 100–350  $mM^{-1}s^{-1}$ , depending upon the number of inner-sphere water exchange sites.<sup>13</sup> However, those systems have not been applied *in vivo* yet so we chose to test our predictions using rather standard polymeric structures based upon the clinically proven  $Gd^{3+}$ -polyamino-polycarboxylate complexes. One could easily achieve a relaxivity of 100  $mM^{-1}s^{-1}$  by multiplexing four  $q=1$   $Gd^{3+}$  complexes together so that each  $Gd^{3+}$  center contributes 25  $mM^{-1}s^{-1}$  to the molecular relaxivity. Perhaps even easier would be to multiplex eight complexes together each having a relaxivity of 12.5  $mM^{-1}s^{-1}$ . This is relatively easy to achieve using simple  $q=1$  complexes. Given these predictions, we proceeded to prepare a small lysine-based dendron consisting of eight individual GdDOTA units each having a  $r_1$  of  $12.3 \pm 0.5 mM^{-1}s^{-1}$  (37°C, pH 7, 23 MHz) per Gd atom (Figure 1). To provide specificity, the dendron was covalently attached to a dimeric peptoid that binds with high specificity and affinity to the vascular endothelial growth factor receptor 2 (VEGFR-2),<sup>14</sup> an important target in tumor metastasis. The  $r_1$  of the  $Gd_8$ -dendron-peptoid conjugate increased to only  $15.1 \pm 0.2 mM^{-1}s^{-1}$  per  $Gd^{3+}$  when fully bound to the VEGFR-2 on agarose beads indicating that the GdDOTA units have considerable motional freedom while bound to the receptor. Nevertheless, this corresponds to a molecular  $r_1$  of 120  $mM^{-1}s^{-1}$  per targeted  $Gd_8$ -dendron-peptoid conjugate. With this system in hand, we then tested whether the predicted detection limits determined for the receptor on agarose beads could be reached in cells with known amounts of the VEGFR-2 receptor on their surface. Porcine aortic endothelial cells with overexpressed human VEGFR-2 (PAE/KDR) ( $2.5 \times 10^5$  receptors per cell) were used for imaging. This corresponded to a receptor concentration per cell (~5  $\mu m$  cell radius) of about 790 nM, near the limit of detection predicted in reference<sup>12</sup>.

PAE/KDR cells were exposed to 1  $\mu M$   $Gd_8$ -dendron-peptoid in phosphate buffered saline (PBS) for 30 minutes at 4°C followed by imaging.  $T_1$ -weighted images of cells exposed to the agent (Figure 2 bottom-right) compared to non-exposed control cells (Figure 2 bottom-left)

were brighter, consistent with agent binding. Given the known binding constant of this targeted agent to the VEGFR2 receptor, one can estimate that the local concentration of bound agent in this experiment was 650 nM with cells exposed to 1  $\mu$ M Gd<sub>8</sub>-dendron-peptoid (agent in excess above the receptor concentration). An ICP-MS analysis of Gd<sup>3+</sup> in the pelleted cells gave a measure value of ~700 nM, in agreement with the known receptor concentration. Although further details should be addressed, it is important to note that this very low sub-micromolar concentration in cells or in solution (Figure 2 top-right) can be detected by MRI as predicted by theory using a relatively simple agent with a molecular relaxivity of only 120 mM<sup>-1</sup>s<sup>-1</sup>.

## Gd<sup>3+</sup> agents that respond to tissue biochemistry – metabolic imaging agents

Our long-term interest in developing MR methods to monitor tissue metabolism *in vivo* has led us to think about the design of contrast agents that respond to important metabolic indices such as tissue pH, tissue redox, hypoxia and metabolite levels. How do the requirements differ for these applications in comparison to those described above for antigen-targeted Gd<sup>3+</sup>-based  $T_1$  agents? First, biological indices such as pH, redox, and pO<sub>2</sub> are a bulk property of tissue so the requirement of high relaxivity is not as important here. More important is the change in relaxivity ( $\Delta r_1$ ) that occurs in response to the metabolic parameter one wishes to monitor by MRI. For example, pH is an important index of metabolism in tissues because excess acid is a hallmark of abnormal metabolism in ischemic tissues, in certain secretory cells, and is certainly important in tumor growth and metastases. Numerous basic publications have reported different designs for pH sensitive Gd<sup>3+</sup>-based  $T_1$  agents<sup>15</sup> but only a few of these have been applied *in vivo*. Thus, we will limit our discussions here to those few examples.

The  $T_1$  relaxivity of a Gd<sup>3+</sup> complex is primarily determined by three factors:  $q$ , the number of water molecules in the inner coordination sphere of Gd<sup>3+</sup>,  $\tau_M$ , the residence lifetime of these inner-sphere water molecules (how fast they are exchanging with other bulk water molecules) and  $\tau_R$ , the rotational correlation time of the agent (how fast the complex tumbles in solution). To prepare a Gd<sup>3+</sup>-based pH sensor then, one only requires a chemical system wherein one or more of these variables ( $q$ ,  $\tau_M$  or  $\tau_R$ ) changes with pH. Examples of all three types can be found in the literature.<sup>16–18</sup> However, the only design that has ever been applied in tissues (perfused tissues or organs or *in vivo*) is GdDOTA-4AmP<sup>5-</sup> (see structure in Figure 3), an agent that responds to pH by changes in proton exchange rate (variable  $\tau_M$ ). This agent is unusual because the single inner-sphere water molecule is actually exchanging quite slowly in this complex ( $\tau_M = 26 \mu$ s) compared to typical clinical Gd<sup>3+</sup> agents (where  $\tau_M$  is typically  $\approx 100 - 200$  ns). However, this complex has four appended phosphonate groups that have pK<sub>a</sub>'s in the range 6.5 to 8 and as these phosphonate groups become protonated below pH  $\approx 8$ , the mono-protonated phosphonate groups hydrogen bond with the single Gd<sup>3+</sup>-bound water molecule and catalytically exchange the highly relaxed bound water protons with protons of bulk water.<sup>19</sup> This has the same effect as an increase in water exchange rate at lower pH values even though the actual rate of water molecule exchange is not affected by changes in pH in this complex. Although this represents a rather unusual mechanism for Gd<sup>3+</sup>-based pH sensor, it should not be surprising that this acid-base catalytic system works so well *in vivo* because acid-base catalysis is a hallmark of many common enzymatic mechanisms in biochemistry.

A major obstacle in applying such systems to image tissue pH is the unknown concentration of the agent in tissue. The measured  $T_1$  contrast of course depends upon two factors, the tissue concentration and the  $r_1$  relaxivity (the pH dependent parameter). Given that one cannot assume the agent concentration is uniform throughout all tissues and furthermore may be changing with time, any measure of absolute pH requires a correction for any gradient in agent concentration at the moment the image is collected. Aime, *et al.*,<sup>20</sup> have pointed out that the ratio,  $R_{2p}/R_{1p}$ , of water protons becomes independent of Gd<sup>3+</sup> concentration for a motionally

restricted agent ( $\tau_R > 1$  ns) but remains dependent on  $\tau_M$ ,  $\tau_R$  and other magnetic parameters that normally affect relaxation in these complexes. They validated the method by demonstrating that the  $R_{1p}$  of aqueous samples containing (GdDOTA)<sub>33</sub>-poly-L-ornithine was sensitive to pH due to a conversion of the poly-L-ornithine from a random structure at high pH values to a more ordered helical structure at lower pH values while  $R_{2p}$  remains independent of pH. Thus, the  $R_{2p}/R_{1p}$  ratio is independent of agent concentration (at least at concentrations high enough to affect these parameters) but is also sensitive to pH, the parameter of interest. While this method is intriguing, the sensitivity of  $R_{2p}/R_{1p}$  to change in pH is relatively small and this may make it difficult to apply *in vivo*.

We have taken a somewhat different approach to image tissue pH by using two Gd<sup>3+</sup>-based agents with similar chemical characteristics (size and charge), one having a  $T_1$  relaxivity that is independent of pH and one having a pH dependent relaxivity. The chemical structures of two such compounds are shown in Figure 3. The  $r_1$  relaxivity of GdDOTP<sup>5-</sup> is insensitive to changes in pH over a wide range while the  $r_1$  relaxivity of GdDOTA-4AmP<sup>5-</sup> changes a modest amount, from 3.5 mM<sup>-1</sup>s<sup>-1</sup> at pH 9.5 to 5.3 mM<sup>-1</sup>s<sup>-1</sup> at pH 6.3 (see Figure 3 and Figure 5).  $T_1$ -weighted dynamic contrast enhanced (DCE) images collected after a bolus injection of one agent followed by images collected after a bolus injection of the second agent provided the data needed to map tissue pH. By making an assumption that the two compounds have identical pharmacokinetics and tissue biodistributions, the image intensity differences at the maximum in the DCE curves may be used to estimate tissue pH. This “dual injection method” has been used to map extracellular tissue pH (pH<sub>e</sub>) mouse kidney<sup>21,22</sup> and in a rat brain glioma (Figure 3).<sup>23</sup> In the glioma model, an intriguing insight provided by the dual injection method includes observation of an inverse relationship between the time-to-maximal intensity (TMI) and pH<sub>e</sub> (Figure 3). This indicates that observation of a larger TMI, indicative of slower perfusion in that tumor, was correlated with lower pH<sub>e</sub> values.

Although this method works quite well *in vivo*, there are some drawbacks to the successive injections of two different agents. During the course of the injections, prolonged exposure to anesthesia may alter the blood pressure, which can result in significant differences in the TMI in the two injections.<sup>23</sup> In addition, there is a temporal price to pay for two injections. It is necessary to wait until most of the contrast agent has exited the tumor before administering the second injection. These considerations make a case for the development of single injection method, which would enhance the clinical utility of a pH<sub>e</sub> sensitive contrast agent.

In many cases, it may not be necessary to measure absolute tissue pH to obtain diagnostically useful information. For example, if the goal is to detect abnormal pH regions of tissues, one might be able to expose the tissue to a pH sensor at a low enough concentration so that significant contrast effects are detected only if tissue pH is abnormally low (assuming the relaxivity increases at lower pH values as with GdDOTA-4AmP<sup>5-</sup>). Some disease processes such as malignancies may produce local increases in both extracellular volume and [H<sup>+</sup>] perhaps improving the threshold for early detection of a cancer or metastasis with water soluble, low molecular weight agents. To illustrate the simplicity of the method, we exposed two different perfused tissue preparations, ischemic rat hearts and pancreatic islets, to GdDOTA-4AmP<sup>5-</sup> and collected  $T_1$ -weighted images (Figure 4A). Normoxic hearts perfused with 100  $\mu$ M agent showed little to no contrast changes after addition of the agent while ischemic hearts showed regions of brightness which we attribute to regions of lower pH in ischemic regions generated during the hypoxic period. Similarly, rat islets embedded in agarose beads and perfused with 50  $\mu$ M GdDOTA-4AmP<sup>5-</sup> showed little  $T_1$  enhancement until the islets were exposed to high concentrations of glucose to promote glucose stimulated insulin secretion (GSIS). Export of insulin from islets is known to be accompanied by release of protons and Zn<sup>2+</sup> ions from insulin granules. This local increase in proton concentration was easily detected as a change in  $T_1$  after exposure of islets to glucose (Figure 4B). This relatively



simple technology offers the opportunity to develop functional assays of islet biology *in vivo*.

Clearly, this simplified approach would work even better if  $\Delta r_1$ , the difference in  $r_1$  between physiological pH and more acidic pH values, was even larger than that displayed by GdDOTA-4AmP<sup>5-</sup>. Standard theory predicts that the  $r_1$  of a Gd<sup>3+</sup> complex undergoing fast water exchange will increase upon slowing molecular rotation or tumbling of the molecule in solution (increasing  $\tau_R$ ). However, GdDOTA-4AmP<sup>5-</sup> is a bit unusual in this context because it has a slowly exchanging water molecule at high pH and a catalytically enhanced proton exchange rate at lower pH values. Based on simple theory, one would predict that the  $r_1$  of the low pH species may become more magnified upon slowing molecular rotation than the  $r_1$  of the slow water exchange species at higher pH. If correct, then  $\Delta r_1$  could be significantly better for a motionally restricted version of GdDOTA-4AmP<sup>5-</sup>. To test this, a bifunctional derivative of GdDOTA-4AmP<sup>5-</sup> was synthesized and reacted with a generation five G5-PAMAM dendrimer having 128 surface amino groups. The product contained on average 96 molecules of benzyl-GdDOTA-4AmP<sup>5-</sup> on the surface of the dendrimer and the resulting macromolecule had an average hydrodynamic volume consistent with a molecular weight of ~140 kD.<sup>19</sup> As anticipated, the  $r_1$  of resulting macromolecular sensor remained pH sensitive (Figure 5) with  $r_1$  increasing from 10.8 mM<sup>-1</sup>s<sup>-1</sup> per Gd<sup>3+</sup> at pH 9.5 to 24.0 mM<sup>-1</sup>s<sup>-1</sup> per Gd<sup>3+</sup> at pH 6. On a macromolecular basis, this corresponds to a change in  $r_1$  from 1037 mM<sup>-1</sup>s<sup>-1</sup> at pH 9.5 to 2304 mM<sup>-1</sup>s<sup>-1</sup> at pH 6. Thus,  $\Delta r_1$  for the dendrimer increased 2.2-fold over this pH range in comparison to a  $\Delta r_1$  of 1.5-fold for monomeric sensor over an identical pH range. This increase was significant but not as large as anticipated. It should be pointed out that the mobility of the dendrimer itself is known to be pH-dependent<sup>24</sup> so part of the change in relaxivity observed in this system may be due to pH-dependent changes in molecular motion of the dendrimer itself and may not solely reflect the pH sensor attached to its surface. Nevertheless, these data show that one could use significantly less pH sensitive dendrimer ( $\approx 0.1 - 0.3 \mu\text{M}$ ) to detect similar changes in pH by MRI as those demonstrated in Figure 4. This experiment has not yet been performed *in vivo*.

## Chemical exchange saturation transfer (CEST) agents

What other methods might be used to image abnormal pH regions in tissues *in vivo*? Ward, et al. were first to demonstrate that image contrast can be altered by taking advantage of chemical species that exchange protons with bulk water via a chemical exchange saturation transfer (CEST) mechanism.<sup>25</sup> Typically, -NH protons in molecules are known to exchange more slowly at low pH than at high pH due to base catalysis of proton exchange so if the rate of exchange,  $k_{\text{ex}}$ , is comparable to the chemical shift difference between the exchanging proton and bulk water ( $\Delta\omega$ ), then application of a frequency-selective presaturation pulse at the chemical exchange site prior to collection of an image will result in chemical transfer of some saturated spins into the water pool, thereby reducing the total amount of water detected in the imaging experiment. The amount of chemically transferred spins of course depends upon several factors including  $k_{\text{ex}}$ , bulk water  $T_1$ , applied B<sub>1</sub> power, and concentration of CEST agent.<sup>26,27</sup> These features make CEST agents unique among the MRI contrast agents in that contrast is generated only when a presaturation pulse at the correct frequency of the chemical exchange site is applied. This means that image contrast may be manipulated by the operator! To obtain a CEST image, one collects two images, one after presaturation at the exchange site of interest and another at an equivalent frequency offset on the opposite side of bulk water. The difference between these two image intensities reports the effects of the exchanging CEST species.

A classic example of pH-dependent -NH proton exchange and its relationship to CEST imaging is given by the work of McMahon, et al.,<sup>28</sup> summarized in Figure 6. These data illustrate the

influence of a increased rate of  $-NH$  proton exchange catalyzed by base on the high resolution  $^1H$  NMR spectrum of poly-L-lysine (left) and the corresponding Z-spectra or CEST spectra (right). At pH 6,  $-NH$  proton exchange is rather slow ( $50\text{ s}^{-1}$ ) and this results in a sharp  $-NH$  proton resonance but a rather small CEST effect (top curve in right panel) but at pH 7.9 where  $-NH$  proton exchange was increased to  $1250\text{ s}^{-1}$ , the high resolution  $^1H$  resonance broadens and almost disappears into the baseline while CEST is larger (bottom curve in the right panel). This trend would continue at even higher pH values until exchange becomes too fast ( $k_{ex} \gg \Delta\omega$ ) and the CEST effect would once again disappear. This pH dependent effect then becomes the basis of using endogenous proteins that have a large number and variety of different  $-NH$  protons to detect changes in tissue pH by CEST imaging.

The first published example of using protein  $-NH$  exchange groups as an endogenous CEST reporter was given by the work of Zhou, et al.<sup>29</sup> Given that the difference in chemical shift between the endogenous  $-NH$  proton resonances and bulk water ( $\Delta\omega$ ) is relatively small (on the order of 3 ppm) and the water proton linewidth *in vivo* is considerably broader than that seen in Figure 6, it becomes necessary to perform an asymmetry analysis to separate out the proton chemical exchange effects from the effects of indirect saturation of water itself.<sup>30</sup> Such analyses are further complicated by the magnetization transfer (MT) effects characteristic of tissues whereby dipolar interactions between water molecules associated with semi-solid macromolecules lead to a broad underlying resonance beneath the bulk water resonance. Given the assumption that the contribution of tissue MT is symmetric about the water resonance, collection of two images with a pre-saturation pulse applied at equal offset frequencies on each side of the bulk water resonance should in principle cancel out the MT contribution plus any contribution due to indirect saturation of water itself, leaving only the effects due to CEST. Even though these combined effects can be substantial, Zhou, et al. were able to detect an ischemic region in brain where the pH was substantially lower than in the surrounding tissues (Figure 7). In this case, the ischemic region is dark because  $-NH$  exchange from endogenous proteins is too slow to detect a CEST effect in those regions where the pH is below 6 or so while the surrounding healthier tissues have a CEST contribution due to  $-NH$  proton exchange. The corresponding histological tissue stain confirmed the result reported by CEST imaging.

The paramagnetic lanthanide ions (other than  $Gd^{3+}$ ) complexed by ligands with exchangeable protons also hold promise as exogenous CEST agents. Given the remarkable hyperfine shifting capabilities of the paramagnetic lanthanide ions, proton ( $-NH$  or  $-OH$ ) or water molecule exchange sites in these complexes are typically frequency-shifted well away from the bulk water resonance ( $\Delta\omega$ ) thereby making direct saturation at those sites considerably more distinct than activation of CEST exchange sites near the bulk water frequency. The resulting PARACEST agents have another advantage in that exchange can be faster while maintaining the intermediate-to-slow exchange condition required for CEST,  $\Delta\omega \approx k_{ex}$ . These agents have not been used to measure pH *in vivo* at this point but they do hold promise for nontraditional imaging objectives such as tomographic images of temperature<sup>31</sup> and extracellular glucose concentrations in tissues.<sup>32,33</sup> Images of temperature or temperature gradients would have numerous applications in medicine and physiology because of the fundamental interactions among heat production, metabolism, blood flow and inflammation, and glucose imaging would be highly relevant to studies of nutrition and diabetes. As pH sensors, PARACEST agents do offer potential advantages over  $Gd^{3+}$ -based agents that require infusion of two compounds to correct for any tissue concentration. One approach to this problem first described by Terreno *et al.*<sup>26</sup> is to build into the same molecule two exchange sites, one insensitive to pH and another sensitive to pH. This was illustrated by the agent  $PrDOTA-(gly)_4^-$  (Figure 8), a complex where water exchange is independent of pH (except for at the extremes of high and low pH) while CEST from the  $-NH$  protons displays a similar pH responsive profile as with other diamagnetic amide  $-NH$  protons. In principle then a pH map of tissues could be obtained after infusion of the single agent followed by CEST measurements using two different presaturation

frequencies, the ratio of which would be a direct readout of pH. Unfortunately, this agent has not yet been tested *in vivo*.

A third generation G3-dendrimer conjugated with sixteen copies of YbDOTAM to increase the sensitivity of CEST was also recently reported (Figure 9).<sup>34</sup> This yielded a molecular system with 48 exchangeable –NH protons that reduced the CEST detection limit into the range of 20  $\mu$ M, a considerable improvement over simple PARACEST monomers such as that shown in Figure 9. Interestingly, the pH profile of the –NH exchanging protons differed between the monomer, a G1 dendrimer and the G4 dendrimer, thereby allowing fine tuning of the pH sensitive region over which the agent would be responsive. Additionally, a CEST agent concentration independent method for metabolite determination consisting of applying two different radiofrequencies for pre-saturation has also been reported and proven to work *in vitro* for pH mapping using the dendrimer system.<sup>35</sup> This latter approach might provide the pathway for exogenous CEST agents to reach *in vivo* applications.

## Summary and Outlook

Responsive MRI agents for monitoring metabolism *in vivo* have only recently begun to appear in the literature and only a few have been demonstrated *in vivo* MRI maps of absolute tissue pH can be obtained by using Gd<sup>3+</sup>-based  $T_1$  agents but the experiments are complicated by the requirement of an independent measure of agent concentration in tissues. Various approaches can be taken to simplify the experimental protocol for obtaining an absolute measure of tissue pH but if one is simply willing to accept detection of low pH regions in tissue, then these agents can be quite useful. pH sensors based on CEST are in many ways more versatile because exchange sites can be built into molecules to make them concentration independent. Unfortunately, none of these have been applied *in vivo* at this point. The opportunities to apply clever chemistry to create novel metabolic imaging agents are vast but chemists should be encouraged to go beyond simply reporting *in vitro* examples and establish long-term collaborations with physiologists and imaging experts to see that such agents get applied *in vivo*. We have held a long-term goal of developing a simple MR imaging method to monitor pH in tumors, ischemic heart tissues, and islet function in the clinical setting and encourage other investigators to bring new ideas to the table.

## Acknowledgements

We wish to thank the NIH (CA-115531, CA-126608, DK-058398, RR-02584 and EB-04582) and the Robert A. Welch Foundation (AT-584) for partial support of this work.

## Biography

### Biographical data

**Luis M. De Leon-Rodriguez** was born in Guanajuato, Mexico in 1973. He received his B.S. in chemistry in 1996 from University of Guanajuato and his Ph. D. in chemistry in 2001 from The University of Texas at Dallas. He is a Professor in University of Guanajuato and is currently an Assistant Instructor in the Advanced Imaging Research Center of the UT Southwestern Medical Center. His research interests focus in the synthesis of biospecific agents for molecular imaging as tools for understating and diagnosis of diseases.

**Robert J. Gillies** received his B.S. in biology in 1974 from UC Irvine and his Ph.D. in 1979 from the University of California, Davis, under the supervision of Prof. David W. Deamer. He had a post-doctoral traineeship with Prof. Robert G. Shulman at Yale University, followed by faculty positions in biochemistry at Colorado State University (1982–1988) and the University of Arizona (1988–2008). He is currently vice chair of Radiology (research) and director of



molecular and functional imaging at the H. Lee Moffitt Cancer Center and Research Institute in Tampa, FL.

**Angelo Josue M. Lubag** received his B.S. and M. S. degrees in Chemistry and Agricultural Chemistry/Biochemistry from the University of the Philippines and his Ph.D. from the University of Texas at Dallas in 2005. He is currently a Postdoctoral Research Fellow at the Advanced Imaging Research Center of the UT Southwestern Medical Center working on MR imaging of metabolic and molecular events in cells, tissues and whole animals - including tissue pH changes in the heart and pancreatic islets.

**Craig R. Malloy** received a B.S. in Chemistry from Stanford University and an M.D. from the University of California at San Francisco. He is currently Professor of Internal Medicine and Radiology at the University of Texas Southwestern Medical Center and staff physician at the VA North Texas Health Care System. His research interests include high field MR imaging and spectroscopy, hyperpolarization, and analysis of metabolic pathways in vivo.

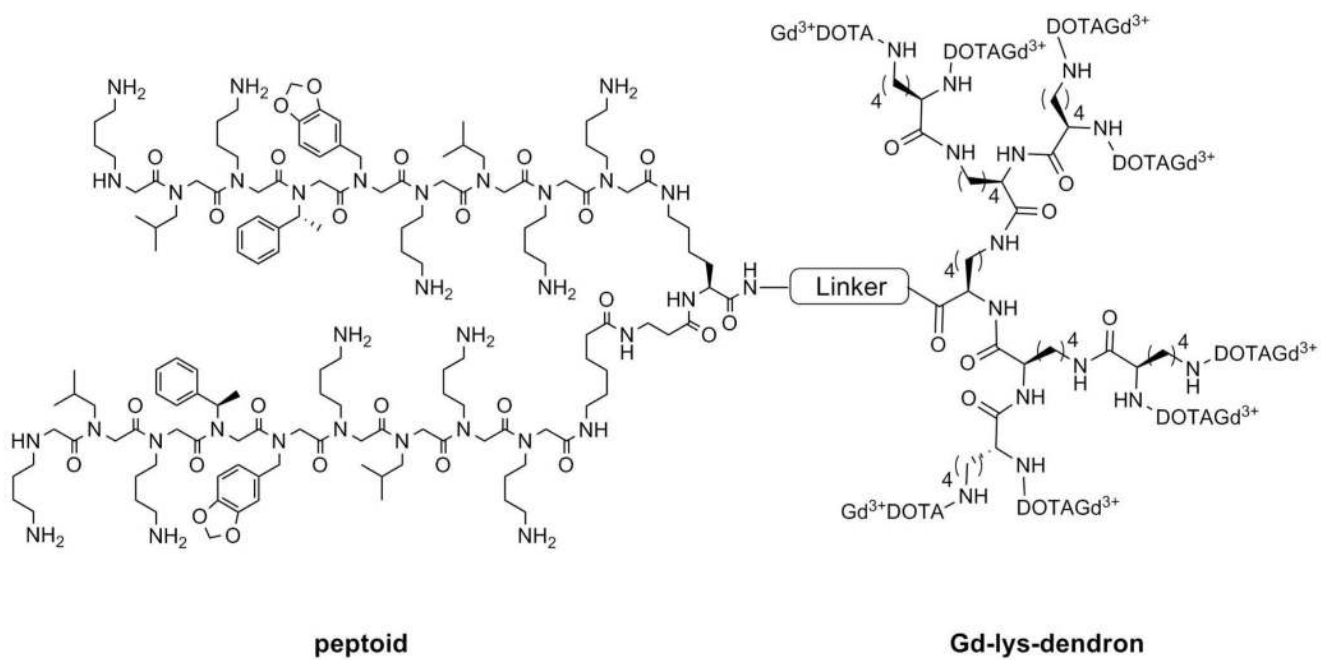
**Gary Martinez** is a senior staff imagine scientist at Moffitt Cancer Center and Research Institute. He received is Ph.D. at the University of California in Santa Cruz under the supervision of Glenn Millhauser (Chemistry). He joined the research group of Robert Gillies in Arizona after a postdoctoral appointment with Prof. S. Wijmenga (Sweden) and NIH NRSA research fellowship with Michael Brown (Arizona). His research interests include in vivo pH measurement with MR and methodological advances in cancer detection, prognosis, and therapy response.

**A. Dean Sherry** received a B.S. in Chemistry from the University of Wisconsin, La Crosse and a Ph.D. in Inorganic Chemistry from Kansas State University in 1967. He was a NIH postdoctoral fellow with Dennis W. Darnell before joining the chemistry faculty at the University of Texas at Dallas in 1972. He currently serves as Director of the Advanced Imaging Research Center on the campus of UT Southwestern Medical Center holds academic appointments at UT Dallas (Chemistry) and UT Southwestern (Radiology). He also holds a Cecil & Ida Green Distinguished Chair in Systems Biology at UT Dallas. His research interests include metabolic imaging agents for MRI,  $^{13}\text{C}$  hyperpolarization studies of intermediary metabolism, and high field MR imaging & spectroscopy.

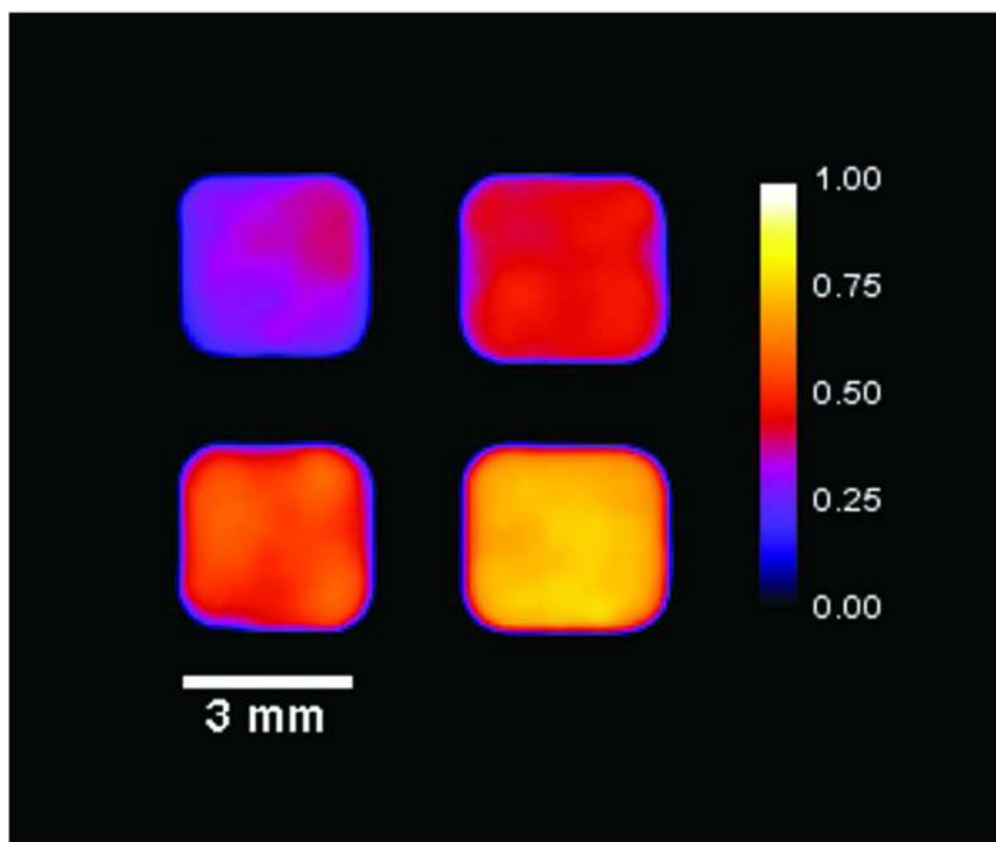
## References

1. Caravan P, Ellison JJ, McMurray TJ, Lauffer RB. Chemical Reviews 1999;99:2293–2352. [PubMed: 11749483]
2. Bellin MF, Eur J. Radiol 2006;60:314–323.
3. Bellin MF, Van Der Molen AJ. Eur. J. Radiol 2008;66:160–167. [PubMed: 18358659]
4. Rooney, WD.; Johnson, G.; Li, X.; Cohen, ER.; Kim, SG.; Ugurbil, K.; Springer, CS, Jr. Magn. Reson. Med. 2007. p. 308-318.
5. Moats RA, Fraser SE, Meade TJ. Angewandte Chemie International Edition in English 1997;36:726–728.
6. Louie AY, Huber MM, Ahrens ET, Rothbacher U, Moats R, Jacobs RE, Fraser SE, Meade TJ. Nat Biotech 2000;18:321–325.
7. Perez JM, O'Loughin T, Simeone FJ, Weissleder R, Josephson L. Journal of the American Chemical Society 2002;124:2856–2857. [PubMed: 11902860]
8. Atanasijevic T, Shusteff M, Fam P, Jasanoff A. Proceedings of the National Academy of Sciences 2006;103:14707–14712.
9. Taktak S, Sosnovik D, Cima MJ, Weissleder R, Josephson L. Analytical Chemistry 2007;79:8863–8869. [PubMed: 17983206]

10. Park I-K, Ng C-P, Wang J, Chu B, Yuan C, Zhang S, Pun SH. *Biomaterials* 2008;29:724–732. [PubMed: 18006052]
11. Bulte JWM, Kraitchman DL. *NMR Biomed* 2004;17:484–499. [PubMed: 15526347]
12. Hanaoka K, Lubag AJ, Castillo-Muzquiz A, Kodadeks T, Sherry AD. *Magn. Reson. Imaging* 2008;26:608–617. [PubMed: 18234462]
13. Jocher CJ, Botta M, Avedano S, Moore EG, Xu J, Aime S, Raymond KN. *Inorg. Chem* 2007;46:4796–4798. [PubMed: 17497773]
14. Udugamasooriya DG, Dineen SP, Brekken RA, Kodadek T. *J. Am. Chem. Soc* 2008;130:5744–5752. [PubMed: 18386897]
15. Aime S, Botta M, Terreno E. *Adv. Inorg. Chem* 2006;57:173–237.
16. Lowe MP, Parker D, Reany O, Aime S, Botta M, Castellano G, Gianolio E, Pagliarin R. *J. Am. Chem. Soc* 2001;123:7601–7609. [PubMed: 11480981]
17. Zhang S, Wu K, Dean Sherry A. *Angew. Chem. Int. Ed. Engl* 1999;38:3192–3194. [PubMed: 10556899]
18. Aime S, Botta M, Crich SG, Giovenzana G, Palmisano G, Sisti M. *Chem. Commun. (Camb.)* 1999:1577–1578.
19. Ali MM, Woods M, Caravan P, Opina AC, Spiller M, Fettinger JC, Sherry AD. *Chem.--Eur. J* 2008;14:7250–7258.
20. Aime S, Fedeli F, Sanino A, Terreno E. *J. Am. Chem. Soc* 2006;128:11326–11327. [PubMed: 16939235]
21. Raghunand N, Howison C, Sherry AD, Zhang S, Gillies RJ. *Magn. Reson. Med* 2003;49:249–257. [PubMed: 12541244]
22. Raghunand N, Zhang S, Sherry AD, Gillies RJ. *Acad. Radiol* 2002;9:S481–S483. [PubMed: 12188315]
23. Garcia-Martin ML, Martinez GV, Raghunand N, Sherry AD, Zhang S, Gillies RJ. *Magn. Reson. Med* 2006;55:309–315. [PubMed: 16402385]
24. Chen W, Tomalia DA, Thomas JL. *Macromolecules* 2000;33:9169–9172.
25. Ward KM, Aletras AH, Balaban RS. *J. Magn. Reson* 2000;143:79–87. [PubMed: 10698648]
26. Terreno E, Castelli DD, Cravotto G, Milone L, Aime S. *Invest. Radiol* 2004;39:235–243. [PubMed: 15021328]
27. Sherry AD, Woods M. *Annual Review of Biomedical Engineering* 2008;10:391–411.
28. McMahon MT, Gilad AA, Zhou J, Sun PZ, Bulte JWM, Van Zijl PCM. *Magn. Reson. Med* 2006;55:836–847. [PubMed: 16506187]
29. Zhou J, Payen JF, Wilson DA, Traystman RJ, Van Zijl PCM. *Nat. Med* 2003;9:1085–1090. [PubMed: 12872167]
30. Zhou J, Van Zijl PCM. *Prog. Nucl. Magn. Reson. Spectrosc* 2006;48:109–136.
31. Zhang S, Malloy CR, Sherry AD. *J. Am. Chem. Soc* 2005;127:17572–17573. [PubMed: 16351064]
32. Trokowski R, Zhang S, Sherry AD. *Bioconjug. Chem* 2004;15:1431–1440. [PubMed: 15546212]
33. Ren J, Trokowski R, Zhang S, Malloy CR, Sherry AD. *Magnetic Resonance in Medicine* 2008;60:1047–1055. [PubMed: 18958853]
34. Pikkemaat JA, Wegh RT, Lamerichs R, van de Molengraaf RA, Langereis S, Burdinski D, Raymond AYT, Janssen HM, de Waal BFM, Willard NP, Meijer EW, Grull H. *Contrast Media Mol. Imaging* 2007;2:229–239. [PubMed: 17937448]
35. Wegh RT, Pikkemaat JA, Willard NP. 2006WO IB51237, 2006114739

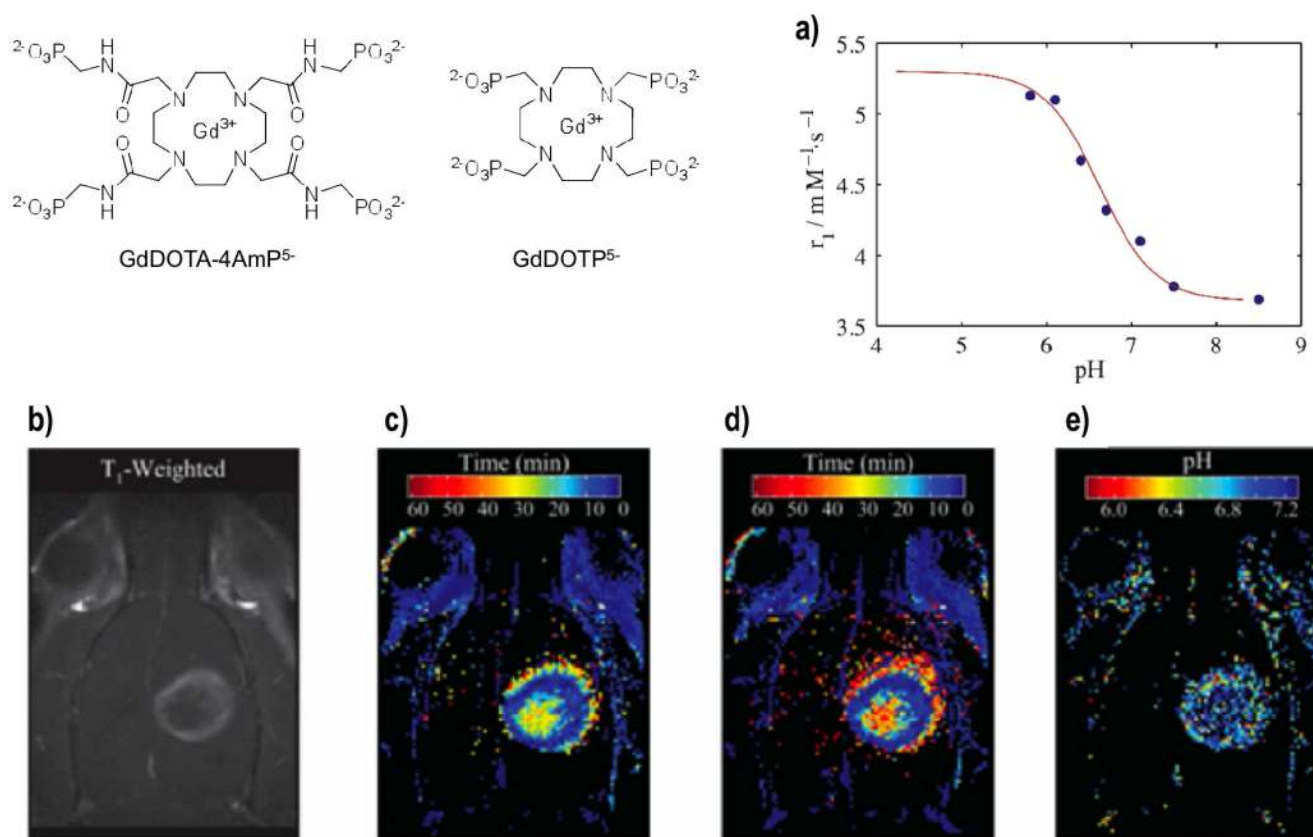


**Figure 1.**  
A Gd<sub>8</sub>-dendron-peptoid used for detection of VEGFR-2 receptors.



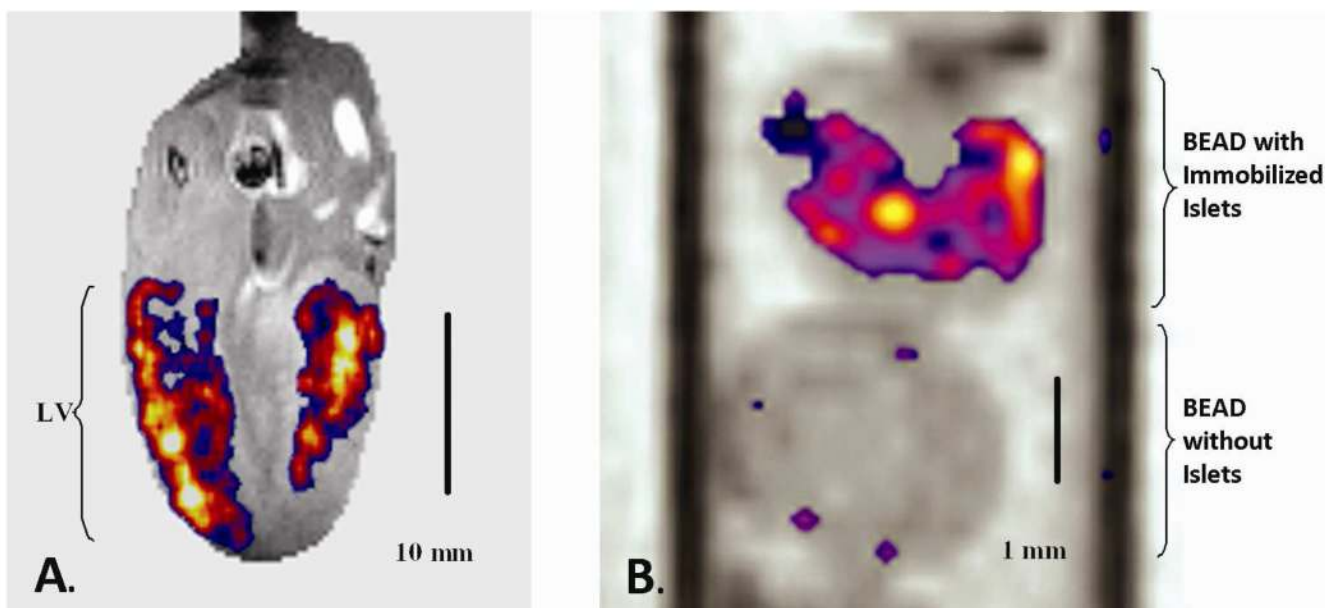
**Figure 2.**

Spin-echo  $T_1$ -weighted coronal MR images of PBS alone (upper-left), 0.5  $\mu\text{M}$  Gd<sub>8</sub>-dendron-peptoid agent in PBS (upper-right), PAE/KDR cells alone without exposure to the agent (lower-left), and PAE/KDR cells exposed to 1  $\mu\text{M}$  agent (lower-right). Conditions: 4.7 T, TR=150 ms, TE=8.5 ms, FOV=30×30 mm, matrix=128×128; ave =12, 2 mm slice, samples in microtiter wells. A 5 pixel radius median filter was applied to the color image shown (Unpublished).

**Figure 3.**

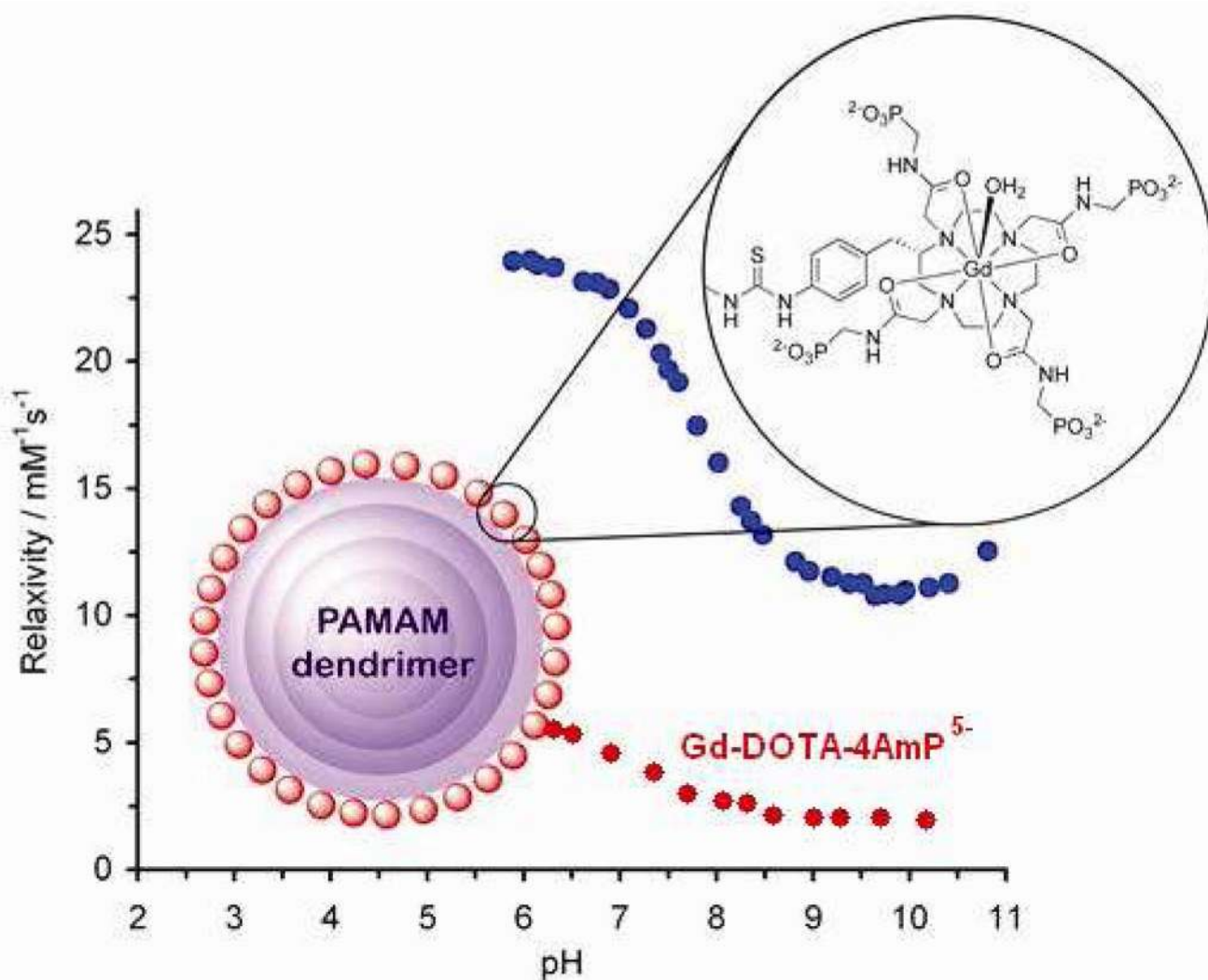
Representative time-to-maximal intensity (TMI) images and the calculated  $pH_e$  map of a C6 glioma in the brain of a live rat. (a) In vitro measurement of  $r_1$  as a function of pH for GdDOTA-4AmP<sup>5-</sup>; (b)  $T_1$ -weighted image of the brain prior to administration of either agent, (c) TMI image after administration of the non-pH sensitive agent, GdDOTP<sup>5-</sup>, (d) TMI image after administration of the pH-sensitive agent, GdDOTA-4AmP<sup>5-</sup>, and (e) the resulting calculated  $pH_e$  image. Reprinted with permission from John Wiley & Sons, Inc: Magnetic Resonance in Medicine,<sup>23</sup> copyright (2006).



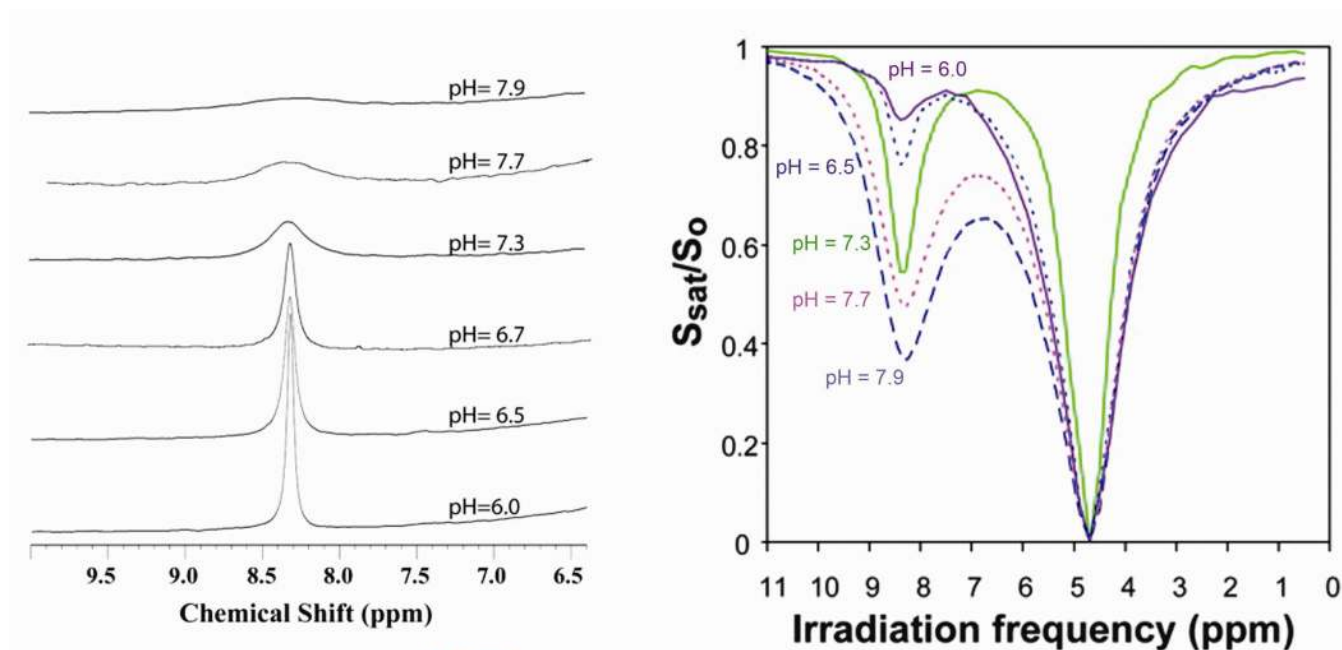


**Figure 4.**

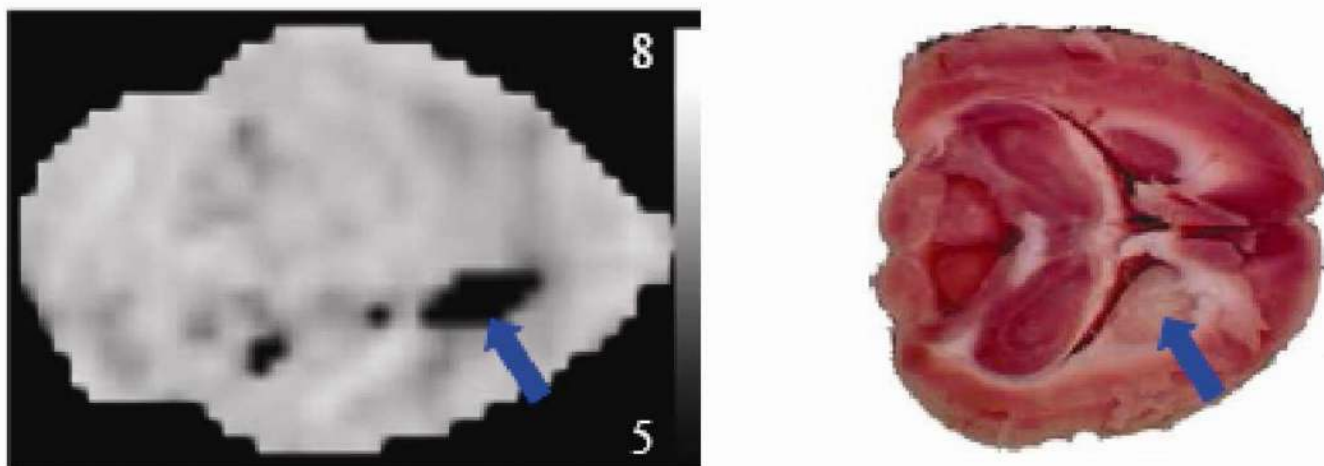
A) MR image of a KCl-arrested rat heart during perfusion with  $100\ \mu\text{M}$  GdDOTA-4AmP<sup>5-</sup> – the gray scale (spin-echo TR300/te8 ms/2mm/128×128/FOV 40×40mm<sup>2</sup>) image shows a single slice through the left ventricular wall while the color overlay reflects the left ventricular muscle regions that became acidic during a 15 minute period of global ischemia (the colorized regions show only those voxels where the signal increased above the noise level due to a decrease in  $T_1$  after ischemia). B) MR image of alginate beads with encapsulated rat pancreatic islets (upper bead; 5% v/v cell-to-bead loading) or an empty bead as control (lower) perfused with  $50\ \mu\text{M}$  GdDOTA-4AmP<sup>5-</sup> – in this case, the color overlay shows only those voxels where the signal increased above noise after the glucose concentration in the perfusate was increased from 5 mM to 25 mM (gradient-echo images, TR8/TE5 ms/ FA=90/1mm/128×256/ave =2/ FOV 20×40 mm<sup>2</sup>) Yellow in the fire-scale color overlays reflect the more acidic regions while purple the less acidic regions. (Unpublished).



**Figure 5.**  $T_1$  relaxivity versus pH profiles for GdDOTA-4AmP $^{5-}$  and a generation-5 PAMAM dendrimer containing 96 molecules of benzyl-GdDOTA-4AmP $^{5-}$  attached to its surface. Reprinted with permission from Wiley-VCH Publishers, Chemistry – A European Journal,<sup>19</sup> copyright (2008)

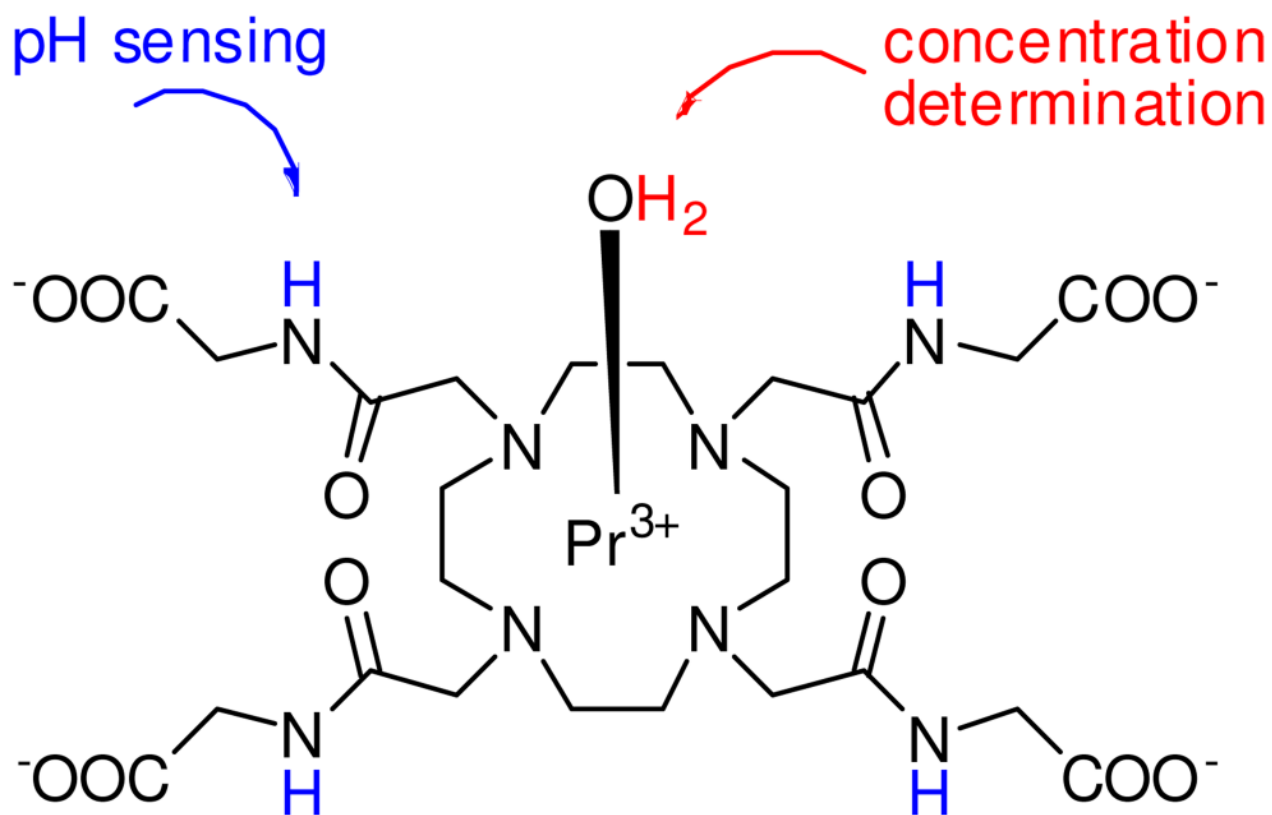


**Figure 6.** High resolution <sup>1</sup>H NMR spectra of the amide protons of poly-L-lysine as a function of solution pH (left) and the corresponding CEST spectra (right). Reprinted with permission from John Wiley & Sons, Inc: Magnetic Resonance in Medicine,<sup>28</sup> copyright (2006).



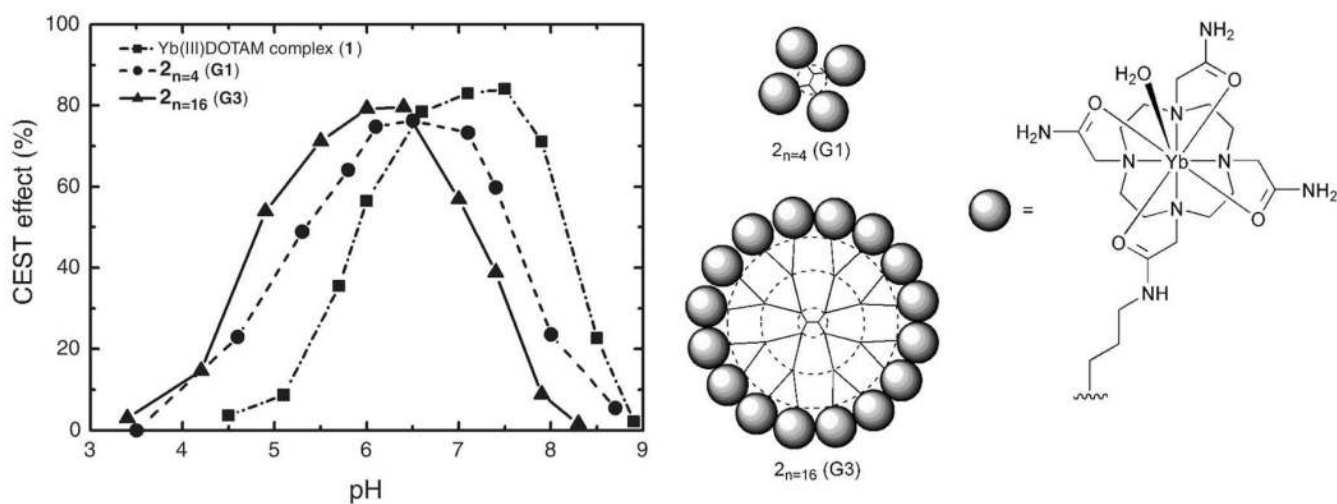
**Figure 7.**

An absolute pH map (left) and the corresponding tissue slice of ischemic rat brain stained with 2,3,5-triphenyltetrazolium chloride. The CEST image was collected at 4.7 T. The area of infarction visible on the right side of both images corresponds to the caudate nucleus (blue arrow), a region commonly affected by infarction following MCA occlusion. Reprinted with permission from Macmillan Publishers Ltd: *Nature Medicine*,<sup>29</sup> copyright (2003).



**Figure 8.**  
PrDOTA-(gly)<sub>4</sub>: A CEST pH sensor with a built-in concentration indicator.



**Figure 9.**

Conjugation of the simple tetraamide complex, YbDOTAM, to dendrimers of various size & generation results in  $-NH$  proton exchange-based CEST agents with differing pH sensitivities. Reprinted with permission from John Wiley & Sons, Inc: Contrast Media and Molecular Imaging,<sup>34</sup> copyright (2007).